SHEATH MOTION IN A CAPACITIVELY
COUPLED RADIO FREQUENCY DISCHARGE

by

B. P. Wood, M. A. Lieberman, and A. J. Lichtenberg

SHEATH MOTION IN A CAPACITIVELY
COUPLED RADIO FREQUENCY DISCHARGE

by

B. P. Wood, M. A. Lieberman, and A. J. Lichtenberg

ELECTRONICS RESEARCH LABORATORY

College of Engineering
University of California, Berkeley
94720

SHEATH MOTION IN A CAPACITIVELY
COUPLED RADIO FREQUENCY DISCHARGE

by

B. P. Wood, M. A. Lieberman, and A. J. Lichtenberg

ELECTRONICS RESEARCH LABORATORY

Sheath Motion in a Capacitively Coupled

Radio Frequency Discharge

B. P. Wood, M. A. Lieberman, and A. J. Lichtenberg

Department of Electrical Engineering and Computer Sciences

and the Electronics Research Laboratory

University of California, Berkeley, CA 94720

ABSTRACT

The sheath motion in a capacitively coupled RF discharge is highly nonlinear. We measure the voltage waveform on a floating probe placed in the sheath region, as a function of position and time. A circuit model of the probe-discharge system relates the observed probe voltage to the sheath motion. The equations derived from this circuit model are solved numerically with varying nonlinear sheath motions; the resulting waveforms are compared with the experimental observations to determine the actual sheath motion. The time-varying plasma potential is also determined, indirectly, from the comparison. We also report observation of oscillations related to the plasma frequency, whose peak harmonic component can be calculated from a simple resonant plasma model. These oscillations can be a useful plasma diagnostic for determining plasma density. The presence of these high frequency oscillations may significantly enhance the rate of stochastic heating of electrons.

1

I. Introduction

Low pressure, capacitively coupled, radio frequency discharges are widely used for materials processing. In such a discharge, the electrons can be thought of as oscillating back and forth between the two electrodes, with nearly all the applied voltage being dropped across the sheaths near the electrodes. The motion of the sheath boundaries are highly nonlinear. The nature of this nonlinearity is important for determining various quantities of interest in the plasma, particularly the stochastic heating of electrons [1–6]. Early r.f. discharge models (for instance, the homogeneous model developed by Godyak and Popov [2,7]) generally assumed that the sheath oscillation was sinusoidal. More recently, Lieberman [5] has provided an analytical, self-consistent solution which predicts a nonlinear sheath motion. Nonlinear sheath motion has also been seen in particle-in-cell discharge simulations [8].

In this paper we describe experimental observations of the voltage waveform produced on a cylindrical Langmuir probe placed in the sheath. We develop a circuit model of the probe-discharge system that relates the observed probe voltage to the motion of the sheath edge. The equations derived from this circuit model are solved numerically, and the resulting waveforms are compared with the experimental observations. In addition, we describe observation of oscillations related to the plasma frequency, and calculate the frequency of the peak harmonic from a simple resonant plasma model.

II. Apparatus

The plasma chamber is an aluminum cylinder one meter long with an inside diameter of 30 cm. Two electrodes, each 23 cm in diameter, are mounted within the chamber on

pistons sealed with two o-rings. One of these electrodes is grounded, as is the chamber itself. The other electrode is connected to an r.f. power source. An electrode spacing of 10 cm was used throughout the experiments. A number of observation and instrumentation ports are spaced around the circumference of the chamber. The chamber is pumped with the standard configuration of a diffusion pump backed by a mechanical pump, giving a base pressure of about 0.01 mTorr. The experiments were performed in argon at a pressure of 3 mTorr, although data to characterize the discharge was taken at a variety of pressures up to 100 mTorr. The r.f. power supply is connected to the powered electrode via a power meter and a matching network, which ensures that power is efficiently coupled to the discharge. All the experiments were performed at 13.6 MHz.

Data are taken with a Stanford Research boxcar gated integrator and recorded on an IBM PC. Data to characterize the discharge density and temperature are taken at a slow rate, about 150 Hz, with a tuned Langmuir probe (described below). Data to characterize the sheath motion are taken at 13.6 MHz, which necessitates a frequency divider to provide a trigger to the boxcar at about 1 KHz. A gate width of 3 ns is used throughout, with each data point being an average over 30 samples.

Data characterizing the plasma density and electron temperature are taken with a tuned Langmuir probe employing a 2 cm length of 2 mil tungsten wire. This probe is connected to a series of parallel LC elements within the probe shaft. These elements are chosen to resonate at 13.6 MHz, so that the probe tip will follow the oscillations of plasma potential. This allows us to analyze the measurements of density and temperature by interpreting the probe I-V characteristic as if it were taken in a d.c. discharge [9]. We find that the r.f. voltage on the powered electrode, $\tilde{V}_{rf}$, varies roughly as the square root of the power over a range

3

of 5-200 watts, and has a value of 220 volts at the operating point of 3 mTorr and 10 watts. Due to the asymmetry of the discharge, the powered electrode (which is capacitively coupled to the r.f. source) takes on a large negative d.c. bias, $\overline{V}_{rf} = -148$ volts. We find that $n_e = 4.1 \times 10^9$ cm^{-3} and $T_e = 4.7$ eV at a point 20 mm from the powered electrode, which is about 4 mm inside the body of the plasma from the sheath edge.

Data characterizing the sheath motion are taken with an un-tuned floating probe consisting of a 20 cm circumference loop of 5 mil tungsten wire placed coaxially to the chamber and with the plane of the loop parallel to the powered electrode. The loop configuration was chosen to yield a signal large in comparison to the r.f. "noise" outside the chamber. About 30 cm of coaxial cable extends from the boxcar to the probe through the glass probe shaft that holds the probe in the chamber. This length of coax, combined with 61 cm of coax inside the boxcar, has a measured total capacitance of 113 pF, which together with the loop probe forms a capacitive voltage divider in the measuring circuit.

III. Circuit Model

A floating probe placed in the sheath behaves to lowest order as a capacitive voltage divider, the two capacitances being that of the probe to the plasma and electrode and that of the probe to the cable and recording device. However, the voltage division is complicated by the nonlinearity of the probe capacitance, sheath motion, plasma potential, and space charge in the sheath. These effects are incorporated in a circuit model of the probe and measurement system. From this model we derive a first-order, nonlinear differential equation that describes the probe potential. This equation is solved numerically for various sheath

4

dynamics to determine predicted waveforms that can be compared with those seen in the experiment.

We first examine the predicted sheath motion from the self-consistent model [5]. The physical situation is shown in Figure 1. Since the ions are massive, and respond only to d.c. fields (f_{pi} in the discharge is about 2 MHz), they form a stationary ion sheath of width s_m. The electrons, with $f_{pe} \approx 575$ MHz, respond instantaneously to the a.c. fields, and form an electron sheath of width x that oscillates between the electrode and s_m. The probe, at a distance d_1 from the electrode, is immersed in the plasma over a portion of the cycle.

The sheath motion was derived analytically in [5] to be:

$$\frac{x}{s_m} = \frac{12}{5\pi H}(1 - \cos \omega t) + \frac{3}{10\pi}\left[\frac{3}{2}\sin \omega t + \frac{11}{18}\sin 3\omega t - \omega t(3\cos \omega t + \frac{1}{3}\cos 3\omega t)\right], \quad (1)$$

where

$$H = \frac{1}{\pi}\left[\frac{12s_m}{5\lambda_d}\right]^{\frac{2}{3}}$$

and λ_d is the electron Debye length. As written here, the origin of the sheath motion ($x = 0$) is at s_m, not at the powered electrode as we have chosen to define it. In the computer code this is easily accounted for by incorporating a phase shift into these equations. The electron density, n_e, begins to fall below the ion density at the point determined from (1), and decreases to zero over some distance characterized by λ_d. Therefore, the actual point at which the electron sheath can be considered to have enveloped the probe lies some number of Debye lengths in front of the point defined by (1). In the computer code we take this into account by considering the effective sheath position to be one Debye length in front of that defined by (1). This value was chosen to produce the best match between simulation and experimental results. The sensitivity of this matching to the number of Debye lengths

5

chosen will be discussed later in this paper. The sheath motion from (1) is shown as the solid line, and the effective sheath edge is shown as the dashed line in Figure 2. The general shape of the time variation of the effective sheath edge resembles that determined by Vender [8] using a particle-in-cell simulation of a similar discharge. The harmonic content in either curve in Figure 2 results in the sheath being near the electrode over a smaller portion of the cycle than would be the case for a pure sinusoid.

The plasma remains positive with respect to the electrode, which takes on a negative d.c. bias in the experiment, so that ions are accelerated across the stationary ion sheath. This results in a decrease in n_i as the electrode is approached, as shown in Figure 3. From this density profile we can determine the net charge density profile, which is then integrated twice numerically in the code to produce the potential profile, normalized to unity, shown in Figure 4. Note that the potential in the sheath is higher than the linear potential variation that would exist in a vacuum sheath.

The circuit model is shown in Figure 5. In this model the a.c. and d.c. voltage sources represent the potential (with respect to ground) in the vicinity of the probe. The two current sources represent the electron and ion conduction currents collected by the probe. R_ℓ is a load resistor attached to the boxcar. In the experiment $R_\ell = 4K\Omega$, which is sufficiently large that the circuit operates approximately as a capacitive voltage divider. Correspondingly, the two most important components of the circuit model are the capacitors C_p, which represents the time-varying capacitance of the sheath around the probe, and C_c, which represents the fixed capacitance of the coax connecting the probe to the boxcar and of the boxcar itself.

6

A set of circuit equations for this circuit model are:

$$i_{Cp} + i_e + i_{ion} = i_{Cc} + i_{R\ell}, \tag{2}$$

where

$$i_{Cp} = C_p \frac{d}{dt}(V_0 - V_p) + (V_0 - V_p)\frac{dC_p}{dt},$$

$$i_e = e n_e A_p \left(\frac{eT_e}{2\pi m_e}\right)^{\frac{1}{2}} e^{(V_p - V_0)/T_e},$$

i_{ion} = constant, depending on probe position,

$$i_{Cc} = C_c \frac{dV_p}{dt}, \tag{3}$$

and

$$i_{R\ell} = \frac{V_p}{R_\ell}.$$

Here V_p is the potential of the probe, V_0 is the potential in the vicinity of the probe, and A_p is the area of the probe. Consistent with the assumption that the circuit operates as a capacitive voltage divider, i_{Cp} and i_{Cc} turn out to be the dominant currents. The conduction currents i_{ion} and i_e are several orders of magnitude smaller than the displacement currents.

There are three different physical environments in which the probe may be found. These are shown in Figure 1 as: (1) in the plasma beyond all sheaths, (2) in the plasma between the electron and ion sheaths, and (3) in both the electron and ion sheaths. Each of these environments produces different equations for V_0 and C_p in the circuit model. We now consider each in detail.

When the probe is in the plasma beyond all sheaths, it sees only the plasma potential, $V_{p\ell} = \overline{V}_{p\ell} + \widetilde{V}_{p\ell}$. The a.c. portion, $\widetilde{V}_{p\ell}$, has been derived in the self-consistent model [5] for a

sinusoidal r.f. current-driven symmetric discharge to be:

$$\tilde{V}_{pl} = \frac{\pi H}{4} T_e \left\{ 4\cos\omega t + \cos 2\omega t + H \left[\frac{5}{3}\pi\cos\omega t \right. \right.$$
$$\left. \left. +\omega t(\frac{3}{8} + \frac{1}{3}\cos 2\omega t + \frac{1}{48}\cos 4\omega t) - \frac{5}{18}\sin 2\omega t - \frac{25}{576}\sin 4\omega t \right] \right\}$$

(4)

This equation is derived assuming that the powered electrode is driven directly by a sinusoidal current source. Our discharge is actually driven by a sinusoidal voltage source through an impedance matching network, but measurements of the resulting r.f. current show it to be very close to sinusoidal. For a non-symmetric, capacitively coupled r.f. discharge, V_{pl} will swing so as to stay positive with respect to the most positive surface in the chamber [10]. In the circuit model, V_{pl} is derived from the total measured voltage on the powered electrode, $V_{rf} = \tilde{V}_{rf} + \overline{V}_{rf}$, by assuming that the plasma must always remain approximately $4KT_e = 19$ volts above both the powered and grounded electrodes. For the experimental discharge in which V_{rf} swings between -368 volts and +72 volts, the plasma potential would then swing between a minimum of 19 volts and a maximum of $72 + 19 = 91$ volts.

With the probe in the plasma beyond all sheaths, C_p is the capacitance across the cylindrical sheath that forms around the probe. The sheath thickness, obtained from the cylindrical Child-Langmuir relation with a Bohm velocity flux of ions [11], is

$$s \approx 0.8\lambda_d \left(\frac{V_{pl} - V_p}{T_e} \right)^{\frac{3}{4}}.$$

(5)

This thickness must be modified to account for the fact that the electrons respond to the time-varying fields. In the planar case, described by the self-consistent model [5], the sheath thickness is increased by a factor of $\sqrt{50/27} \approx 1.36$ over the Child-Langmuir result. We

will assume this factor to be applicable to the cylindrical case as well. We can then use the formula for a coaxial capacitance,

$$C = \frac{2\pi\epsilon_0\ell}{\ln(b/a)},\tag{6}$$

where $b = a + s$ is the radius of the outer conductor (the sheath boundary in this case), to derive an expression for C_p:

$$C_p = \frac{2\pi\epsilon_0\ell}{\ln\left[1 + (1.1\lambda_D/a)\left((V_{pl} - V_p)/T_e\right)^{3/4}\right]}.\tag{7}$$

The ion current in this environment is approximately given (see Chen [12]) by the Bohm presheath value $i_{ion} = 0.6n_i eA_p(eT_e/M)^{1/2}$. Using the expressions for C_p and $V_0 = V_{pl}$, the circuit equations (2) and (3) can be put into the form:

$$\frac{dV_p}{dt} = f\left(V_p, V_{pl}, \frac{dV_{pl}}{dt}\right).\tag{8}$$

When the probe is in the plasma between the electron and ion sheaths we must modify the expressions for C_p and i_{ion} to account for the beam-like quality of the accelerated ions as we get closer to the powered electrode. In the situation where the probe is far enough from the ion sheath boundary that the beam velocity of the ions is much larger than the Bohm velocity, the perturbation of the ions due to the cylindrical electron sheath that forms around the probe will be negligible, and we can assume that n_i is approximately constant in the vicinity of the probe. The Child-Langmuir relation will no longer be valid, but we can calculate the thickness of the cylindrical electron sheath as that distance necessary to drop the potential difference between the probe and plasma through the constant ion density:

$$s = \left[\frac{4\epsilon_0\left(V_{pl} - V_p\right)}{en_i}\right]^{1/2}.\tag{9}$$

9

Using (9) in (6), we find:

$$C_p = \frac{4\pi\epsilon_0 \ell}{\ln\left[4\epsilon_0\left(V_{pl} - V_p\right)/\left(en_i a^2\right)\right]}.$$ (10)

The ion current in this environment is the ion flux striking the cross-sectional area of the probe, $i_{ion} = 2a\ell n_0(eT_e/M)^{1/2}$, where ℓ is the length of the probe [13]. Using the expressions for C_p and $V_0 = V_{pl}$, the circuit equations (2) and (3) can put into the form:

$$\frac{dV_p}{dt} = g\left(V_p, V_{pl}, \frac{dV_{pl}}{dt}\right).$$ (11)

When the probe is in both the electron and ion sheaths, it forms a voltage divider between the potential of the powered electrode and the plasma potential. Letting $V_{rf} = \overline{V}_{rf} + \tilde{V}_{rf}$ be the potential of the powered electrode, the potential at the probe if there is no charge density in the sheath would be:

$$V_0 = \frac{d_1}{x}V_{pl} + \frac{x - d_1}{x}V_{rf}.$$ (12)

This potential must be weighted by the numerically determined potential profile shown in Figure 4, to account for the non-zero charge density en_i in the sheath. In this environment, C_p represents the capacitance of the probe with respect to both the sheath boundary and the powered electrode. Referring to Figure 1, with $a \ll d_1$ and the length of the probe $\ell \gg x$, the resulting capacitance can be calculated (see Morse and Feshbach [14]) to be:

$$C_p \approx \frac{2\pi\epsilon_0 \ell}{\ln\left[\left(\frac{2x}{\pi a}\right)\sin\left(\frac{\pi d_1}{x}\right)\right]}.$$ (13)

Note that this expression for C_p is purely geometrical, and does not depend on the potentials of the probe or plasma. We measured the actual value of C_p with the probe close to the powered electrode in the absence of a discharge. The values we found were roughly half those

calculated by (13). Therefore, in determining C_p in the simulation model, we multiply (13) by 0.5 to bring it into consistency with the experimental observations. The electron current, i_e, is set to zero because $n_e = 0$ in this environment. Using the expressions for C_p and V_0, the circuit equations (2) and (3) can put into the form:

$$\frac{dV_p}{dt} = h\left(V_p, V_{pl}, V_{rf}, x, d_1, \frac{dV_{pl}}{dt}, \frac{dV_{rf}}{dt}, \frac{dx}{dt}\right).$$ (14)

In order to solve the circuit model numerically, we must choose which differential equation to solve. If the probe is in the plasma beyond all sheaths, we apply (8) at all times. If $d_1 < s_m$, we must choose whether to apply (11) or (14) at any particular time. Equation (13) for C_p in the electron and ion sheaths is singular when $d_1 \approx x$, that is, when the electron sheath sweeps by the probe. Figure 6 shows the value of C_p versus the electron sheath position x according to both (13) and (10). Considering the real, physical discharge, it is obvious that C_p should be continuous over all time. This dictates that the transition between the two differential equations be made at the point where the curves in Figure 6 intersect, always choosing the smaller of the two values for C_p. Less obvious, but important for the model due to the $\frac{dC_p}{dt}$ term in (3), is that $\frac{dC_p}{dt}$ should be continuous as well. To see this, consider the physical shape of the electron sheath as it sweeps by the probe. The electron sheath edge will be perturbed when it comes within a few Debye lengths of the probe and can be expected to envelop the probe continuously over a range of positions. Calculating the sheath geometry in these intermediate positions is a difficult free-boundary problem. Rather than tackle this problem, we have chosen to vary C_p smoothly over the range of what would have been the cylindrical sheath thickness around the probe, calculated according to (9).

This smoothed value is shown as the dotted line in Figure 6. This reduces the non-physical large value for $\frac{dC_p}{dt}$ at the transition, and reduces its discontinuity to a negligible value.

Choosing the proper differential equation, the circuit model has been solved numerically, using a fourth-order Runge-Kutta algorithm described by Press, Flannery, Teukolsky, and Vetterling [15].

IV. Sheath Dynamics

The 13.6 MHz waveforms were recorded using the loop probe as a function of distance from the powered electrode, with the discharge operated at 3 mTorr and 10 W. To explore the consistency of the capacitive divider model, measurements were made at values of C_c equal to 113, 200, and 284 pF. The first of these represents the total capacitance of the coax connecting the probe to the boxcar, and the boxcar capacitance itself. The additional capacitance needed to vary C_c was supplied by a silver mica capacitor connected across the coax at the boxcar input. These capacitances were measured at 13.6 MHz and higher harmonics using an HP 8753A Network Analyzer. The boxcar was connected as closely as possible (30 cm) to the probe, since long stretches of unmatched coax set up standing waves that added low order harmonics to the waveform.

The optical emission from the discharge ends abruptly in a dark region near the electrodes. The ion sheath thickness, s_m, was found to be about 15.8 mm, corresponding to both the visible edge of the dark region, and the point at which the spatial variation of the probe signal flattens out. The minimum probe signal occurred at 17.7 mm from the powered electrode. Thereafter the signal increased, reflecting the increasing plasma density toward

the center of the discharge. Measurements were taken every 2.54 mm beginning 5 mm from the powered electrode, until the probe was clearly in the body of the plasma. Figure 7 shows the waveforms recorded for $C_c = 113$ pF and $d_1 = 5.0, 7.5, 10.1, 12.6,$ and 15.2 mm. We discuss the high frequency oscillations that appear in these waveforms later in this paper.

The rms magnitude of the waveforms from the circuit model (solid lines) and experiment (dashed lines) are compared versus the distance d_1 of the probe from the powered electrode in Figure 8. Separate curves are shown for (from the top to the bottom) $C_c = 113, 200,$ and 284 pF, and each curve represents measurements at $d_1 = 5.0, 7.5, 10.1, 12.6, 15.2, 16.4, 17.7,$ and 19.0 mm. The rates of variation with position are weaker for the circuit model than for the experiment, resulting in the circuit model rms value being higher than the experiment when the probe is in the plasma beyond all sheaths. As previously discussed, the peak-to-peak plasma potential is indirectly determined from the relationship that the plasma voltage is at all times $4KT_e$ above the most positive wall potential, resulting in a peak-to-peak plasma potential of 72 volts. This value was used in the simulation model, but may be too simple an assumption. Several authors [16,17] have experimentally found sheath structures which can take the plasma potential close to, or even slightly below, the maximum powered electrode potential. This has been found in particle-in-cell simulations as well [18]. A value of $4KT_e$ is probably a good estimate for the minimum plasma potential above the grounded electrode, so the 72 volt value is may be an overestimate by as much as $4KT_e$. If we match the theoretical and experimental values of probe voltage within the plasma by independently varying the plasma potential, we obtain the results shown in Figure 9. This matching value corresponds to a peak-to-peak oscillation of the plasma potential of 50 volts. Matching the results in this way may be a better method of determining this oscillation amplitude. In

13

both Figure 8 and Figure 9 the electron sheath edge has been advanced by one Debye length, as discussed previously. In Figure 9 we show the effect of this advance on the waveforms. The dotted lines that lie above and below the 113 pF line have no advance and $3\lambda_d$ advance, respectively; λ_d varies from 0.25 mm at the ion sheath edge to 1.0 mm at $d_1 = 5$ mm. The spacing of the curves in Figure 9 indicates the correctness of the capacitive voltage divider model, for which the probe potential is proportional to the ratio of the capacitances:

$$V_p \propto \frac{C_p}{C_p + C_c}.$$
(15)

To determine the detailed shape of the sheath motion we can vary the assumed motion in the model and compare the resultant time-varying probe voltage with that found experimentally. In particular, we compare the experimental result (dotted line) with the result for the self-consistent sheath (solid line), as given in (1), and with the result for a sinusoidal sheath oscillation that corresponds to a uniform ion density in the sheath (dashed line). The resultant waveforms are shown in Figure 10 and Figure 11 for $d_1 = 5$ mm and 12.6 mm, respectively. The waveforms are normalized to give the same magnitude of the fundamental frequency. The 12.6 mm experimental waveform has been filtered to remove a plasma oscillation component between the 9th and 14th harmonics of 13.6 MHz, which will be discussed in the next section. The self-consistent sheath motion produces a waveform which is a better fit to the experimental data than the waveform resulting from the sinusoidal sheath motion. This is particularly evident when the probe is close to the ion sheath edge. Other models of sheath motion can be similarly tested.

V. Plasma Oscillations

The signal picked up by a floating probe has a surprisingly rich harmonic spectrum at frequencies near the electron plasma frequency, f_{pe}. An example of the spectrum from a floating cylindrical probe placed near the ion sheath edge at 10 watts and 3 mTorr is shown in Figure 12. This spectrum is calibrated in dBm, and was taken using an HP 8569B frequency spectrum analyzer. Plasma oscillations of this type have also been seen in particle-in-cell simulations of similar discharges [19]. Note that only discrete harmonics of 13.6 MHz appear, and that the peak harmonics (the 15th and 16th) are of the same magnitude as the fundamental frequency. Other measurements show that the peak harmonics have a lower magnitude with respect to the fundamental frequency when the probe is moved away from the ion sheath edge, either into the plasma or toward the powered electrode. Tuned Langmuir probe measurements indicate that $f_{pe} = 575$ MHz corresponds to the 42nd harmonic in Figure 12. In Figure 13, the frequency of the peak harmonics in the spectrum (squares) are plotted over a range of powers at 3 mTorr, along with the plasma frequency corresponding to the measured density at that power (diamonds). Both sets of data clearly show that the plasma frequency depends upon power as $f_{pe} \propto (\text{power})^{1/4}$. The frequency of the peak harmonic is consistently equal to 0.38 of f_{pe}. This suggests that the frequency of the peak harmonic can be used as a diagnostic to determine n_e.

The factor of 0.38 can be approximately calculated from a simple resonant model of the plasma and sheath. Assume that ℓ_p is the length of the plasma and ℓ_s is the total length of

both sheaths. The discharge can be modeled as two capacitors in series, where

$$C_s = \frac{\epsilon_0}{\ell_s},$$

and (16)

$$C_p = \frac{\epsilon}{\ell_p} = \frac{\epsilon_0(1 - \omega_p{}^2/\omega^2)}{\ell_p}.$$

The total capacitance will be $C_T = (1/C_p + 1/C_s)^{-1}$. Using (16), we find

$$C_T = \frac{\epsilon_0\left(\omega^2 - \omega_p{}^2\right)}{\ell_s\left(\omega^2 - \omega_p{}^2\right) + \ell_p\omega^2}.$$

This expression will be resonant when the denominator vanishes, or

$$\omega = \omega_p\left(\frac{\ell_s}{\ell_s + \ell_p}\right)^{1/2}.$$ (17)

In the experimental discharge, $\ell_s \approx 20$ mm (the sheath near the grounded electrode is only 4-5 mm wide), and the total length $\ell_s + \ell_p = 100$ mm, yielding the relation $\omega \approx 0.45\omega_p$, in reasonable agreement with the experiment.

These oscillations can be seen in the boxcar data as well. Figure 14 shows the experimental waveform (dotted line) and the experimental waveform filtered to include only the $9^{\text{th}} - 14^{\text{th}}$ harmonics with $d_1 = 15.2$ mm. The oscillations are strongest when the sheath is moving fastest. This is also the portion of the cycle in which the moving sheath can deliver the largest kick to stochastically heat electrons. The presence of these large, high frequency oscillations suggests that rates of stochastic heating may be substantially higher than current models predict.

VI. Conclusions

We have investigated the nonlinear motion of the sheaths in a capacitively coupled r.f. discharge by observing the signal from a Langmuir probe placed in the sheath region. These results were compared to a simulation using a circuit model of the system that includes the nonlinear sheath motion, probe capacitance, plasma potential, and space charge in the sheath. The circuit model also uses a number of parameters that were experimentally determined in the discharge.

The magnitudes of the waveforms from the circuit model scale similarly with probe position and measuring circuit capacitance to those from the experiment. The shape of the circuit model waveforms closely approximate those from the experiment when a self-consistent model for the sheath motion [5] is used in the circuit model. Matching the theoretical to the experimental waveform when the probe is imbedded in the plasma can be used as an independent determination of the oscillating plasma potential. The shape of the sheath oscillation can be determined approximately by comparing the resultant theoretical waveforms with those found experimentally. A sinusoidal sheath motion, corresponding to a uniform ion density, non-self-consistent sheath oscillation, is a poorer match to the experiment than that of the self-consistent oscillation.

A simple resonant model of the plasma and sheath can predict the frequency of higher harmonic oscillations near the plasma frequency. The presence of these harmonics can be used as a diagnostic to determine n_e. The large magnitude of these higher harmonics, particularly at the ion sheath edge, suggests that they may be an important factor in the stochastic acceleration of electrons.

17

References

[1] A. I. Akhiezer and A. S. Bakai, Sov. J. Plasma. Phys. $\underline{2}$ 359 (1976).

[2] V. A. Godyak, Sov. J. Plasma Phys. $\underline{2}$ 78 (1976).

[3] O. A. Popov and V. A. Godyak, J. Appl. Phys. $\underline{57}$ 53 (1985).

[4] M. J. Kushner, I.E.E.E. Transactions on Plasma Science, $\underline{14}$ 188 (1986).

[5] M. A. Lieberman, I.E.E.E. Transactions on Plasma Science, $\underline{16}$ 638 (1988).

[6] C. G. Goedde, A. J. Lichtenberg, and M. A. Lieberman, J. Appl. Phys. $\underline{64}$ 4375 (1988).

[7] V. A. Godyak and O. A. Popov, Sov. J. Plasma Phys. $\underline{5}$ 227 (1979).

[8] David Vender and Rod W. Boswell, I.E.E.E. Transactions on Plasma Science, $\underline{18}$ 725 (1990).

[9] R. R. J. Gagne and A. Cantin, J. Appl. Phys. $\underline{43}$ 2639 (1972).

[10] H. R. Kohler, J. W. Coburn, D. E. Horne, E. Kay, and J. H. Keller, J. Appl. Phys. $\underline{57}$ 59 (1985).

[11] William G. Dow, Fundamentals of Engineering Electronics Wiley N.Y. 1937.

[12] Francis F. Chen, Introduction to Plasma Physics and Controlled Fusion vol. 1, second edition, Plenum N.Y. 1984.

[13] I. Langmuir and H. M. Mott-Smith, G. E. Rev. $\underline{27}$ 545 (1924).

[14] Philip M. Morse and Herman Feshbach, Methods of Theoretical Physics McGraw-Hill N. Y. 1953.

[15] William H. Press, Brian P. Flannery, Saul A. Teukolsky, and William T. Vetterling, Numerical Recipes Cambridge University Press, Cambridge 1986.

[16] M. H. Cho, N. Hershkowitz, and T. Intrator, J. Vac. Sci. Technol. A $\underline{6}$ 2978 (1988).

[17] A. H. Sato and M. A. Lieberman, submitted to J. Appl. Phys.

[18] M. V. Alves, V. Vahedi, and C. K. Birdsall, Bull. Am. Phys. Soc. 34 2028 (1989).

[19] J. P. Verboncoeur, V. Vahedi, M. A. Lieberman, and C. K. Birdsall, "Work Done and Energy Balance in RF Discharges", presented at the IEEE International Conference on Plasma Science, May 1990.

Figures

Figure 1. Physical arrangement of the probe in the sheath. The maximum sheath width is also the stationary ion sheath width.

Figure 2. Time variation of the electron sheath width, x, normalized to the maximum electron sheath width, s_m. Zero corresponds to the sheath being at the powered electrode. The solid line is from (1). The dashed line has the sheath advanced by one Debye length.

Figure 3. Ion and electron densities in the sheath. The ion density n_i is reduced near the electrode due to the acceleration of the ions. The electron density $n_e(t)$ follows n_i until reaching the electron sheath edge, at which point it falls to zero within a few Debye lengths.

Figure 4. Normalized potential variation in the sheath, as obtained by twice integrating the charge densities in Figure 3.

Figure 5. Circuit model for the probe-discharge system.

Figure 6. Capacitance C_p calculated from (13) and (10) at a probe position of $d_1 = 10$ mm, with $C_c = 113$ pF. The dotted line shows the ramped value of C_p used by the program to diminish the non-physical discontinuity in $\frac{dC_p}{dt}$.

Figure 7. Probe voltage waveforms recorded on the boxcar for $d_1 = 5.0, 7.5, 10.1, 12.6,$ and 15.2 mm and $C_c = 113$ pF.

Figure 8. Rms probe voltage versus probe position, d_1, from experiment (dashed lines) and circuit model (solid lines). The maximum electron sheath width is 15.8 mm. The sheath has been advanced by one Debye length. From top to bottom, the curves are for cable capacitances $C_c = 113, 200,$ and 284 pF.

Figure 9. Same as Figure 8, but with the plasma potential V_{pl} multiplied by 0.7 to to produce the proper rms magnitude for the waveform when the probe is completely in the plasma. The upper and lower dotted lines show the rms magnitudes when the sheath is not advanced and advanced by $3\lambda_d$, respectively.

Figure 10. Comparison of the circuit model waveforms for the nonlinear sheath motion [5] (solid line) and a sinusoidal sheath motion (dashed line), both advanced by one Debye length. Here $C_c = 113$ pF and $d_1 = 5$ mm. The dotted line is the experimentally observed waveform. The magnitudes of the circuit model waveforms have been adjusted to match those of the experimental waveform, to facilitate comparison of their shapes.

Figure 11. Same as Figure 10, expect that $d_1 = 12.6$ mm.

Figure 12. Frequency spectrum from a floating Langmuir probe placed 20 mm from the powered electrode at 10 watts and 3 mTorr.

Figure 13. Comparison of the frequency of the peak harmonic (squares) with the measured value of f_{pe} (diamonds) versus power. More than one square is shown where there were several peak frequencies of approximately equal magnitude.

Figure 14. Experimental waveform with $d_1 = 15.2$ mm. The dotted line is the complete waveform, and the solid line is produced by filtering all but the $9^{th} - 14^{th}$ harmonics.

Figure 1

Figure 2

Density

n_i

$n_e(t)$

O

$x_s(t)$

Oscillating
Electron
Sheath

s_m

Max Sheath
Thickness

Figure 3

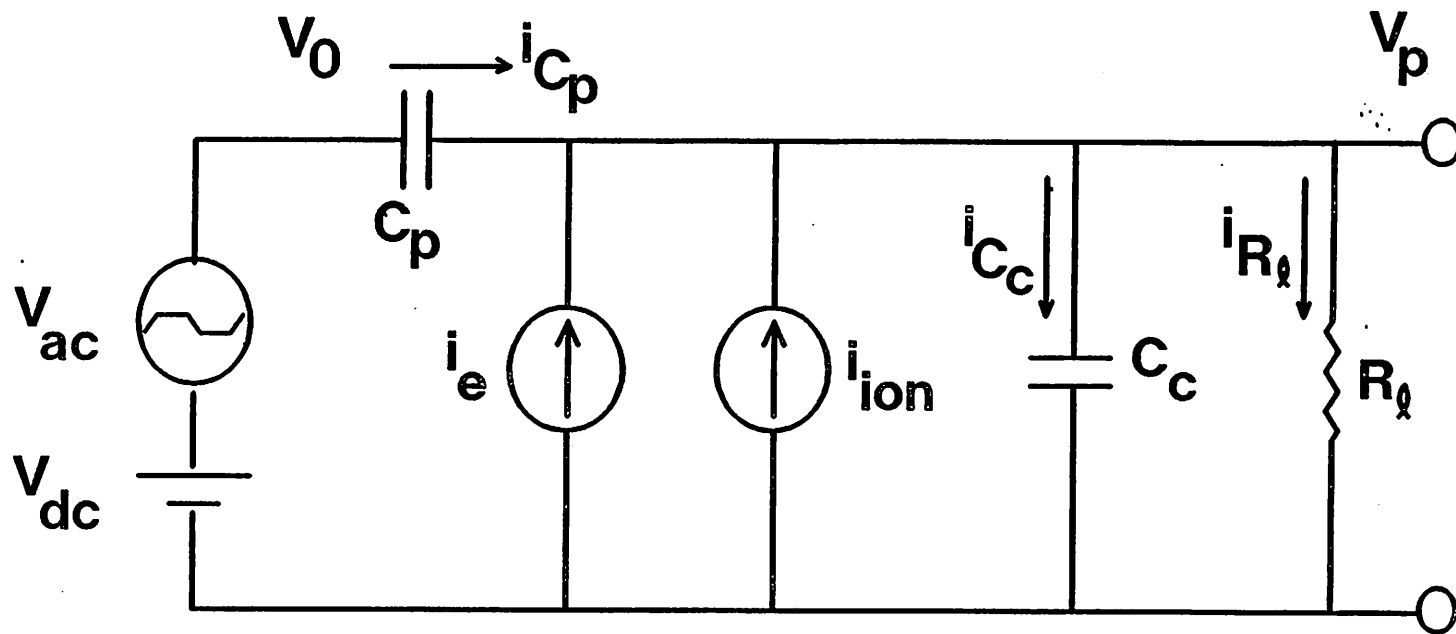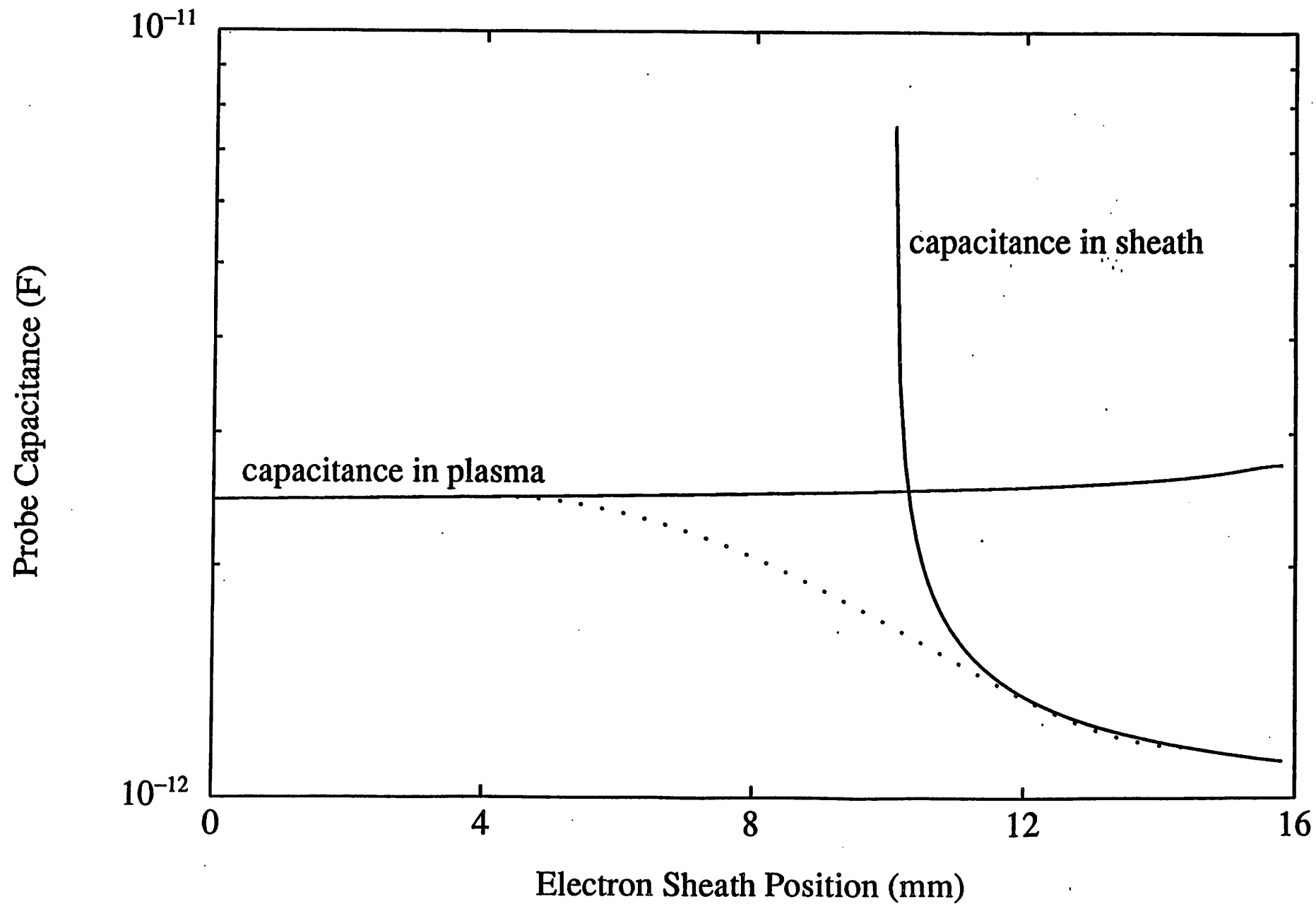**Potential**

O

$x_s(t)$

Oscillating
Electron
Sheath

s_m

Max Sheath
Thickness
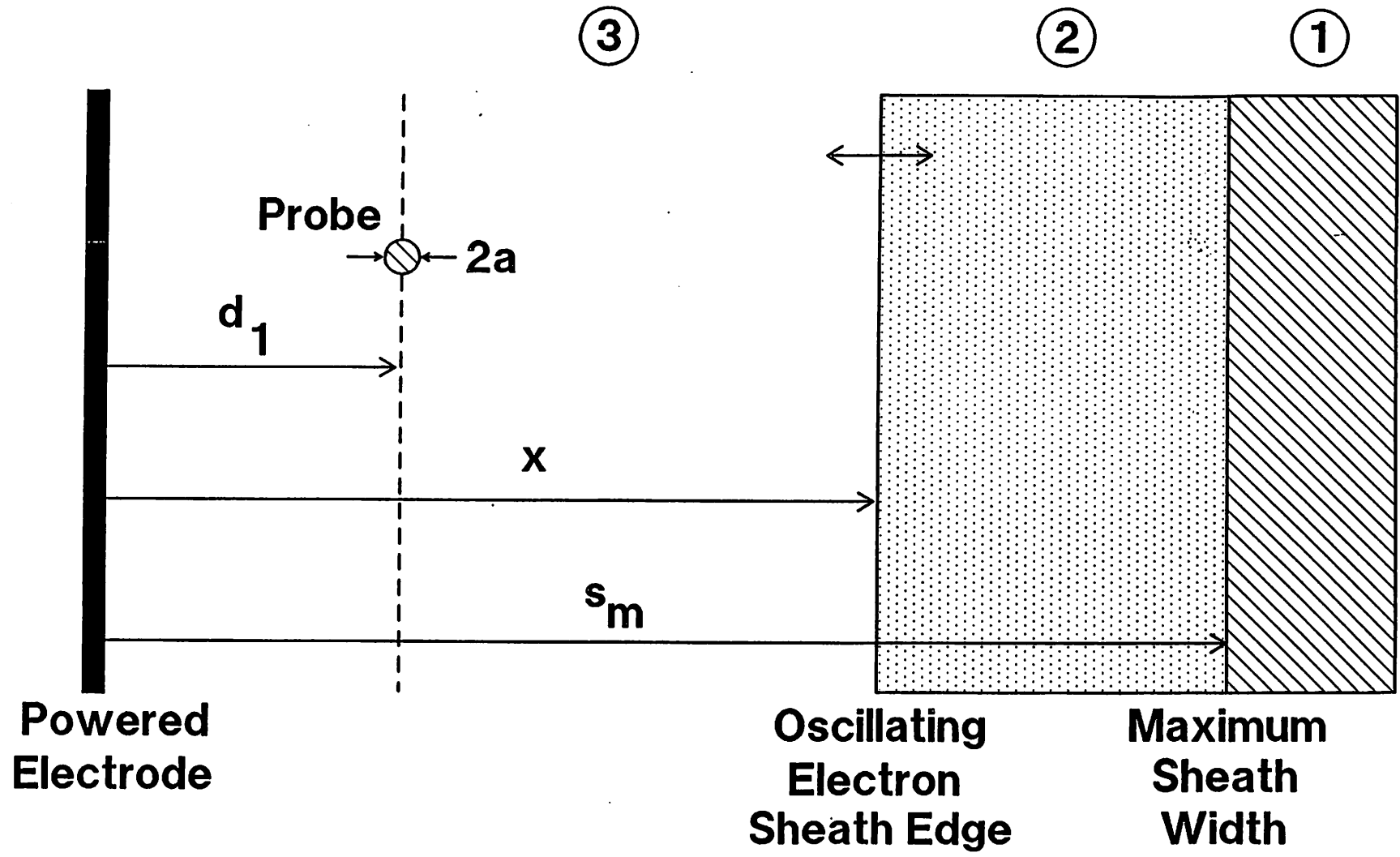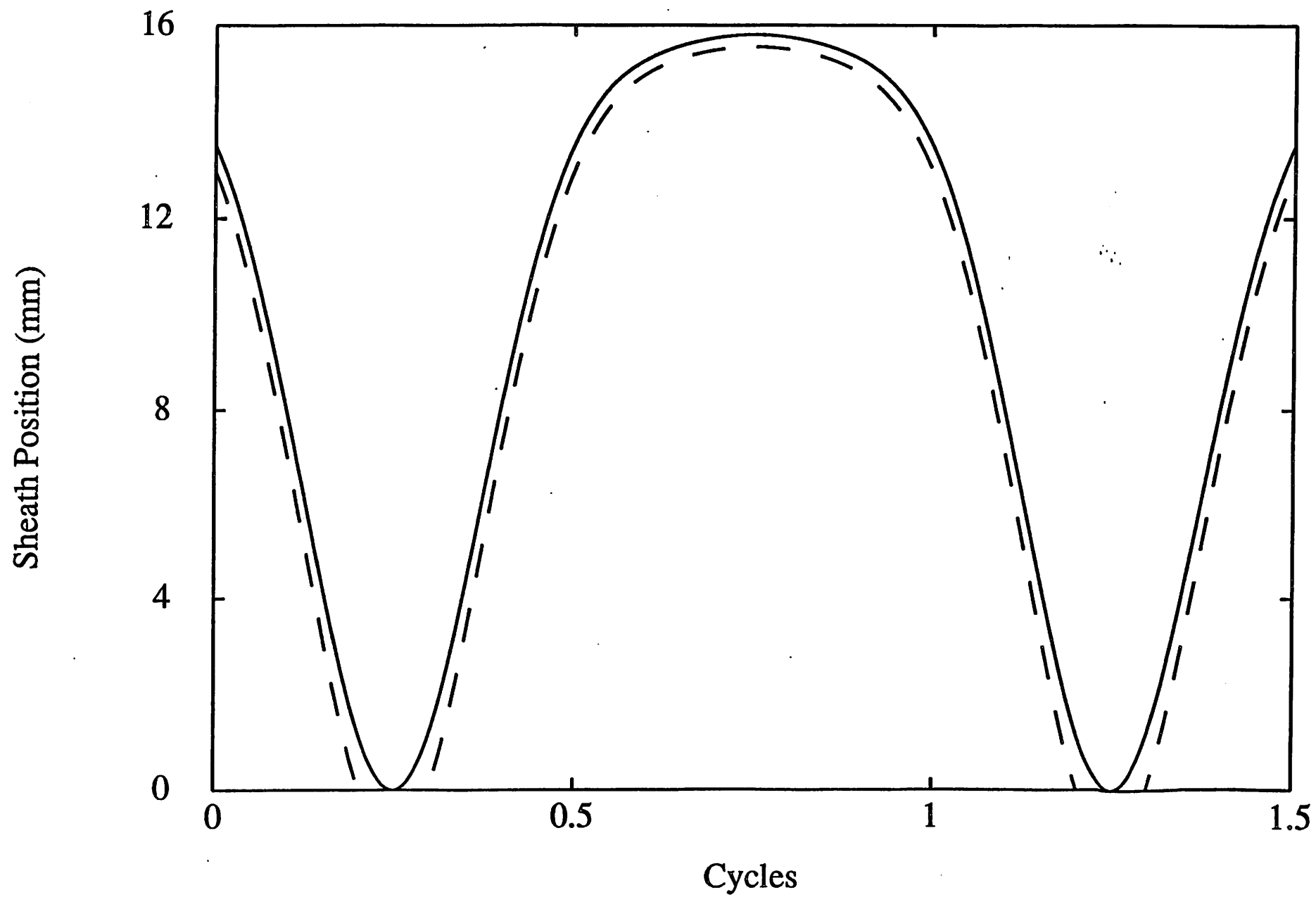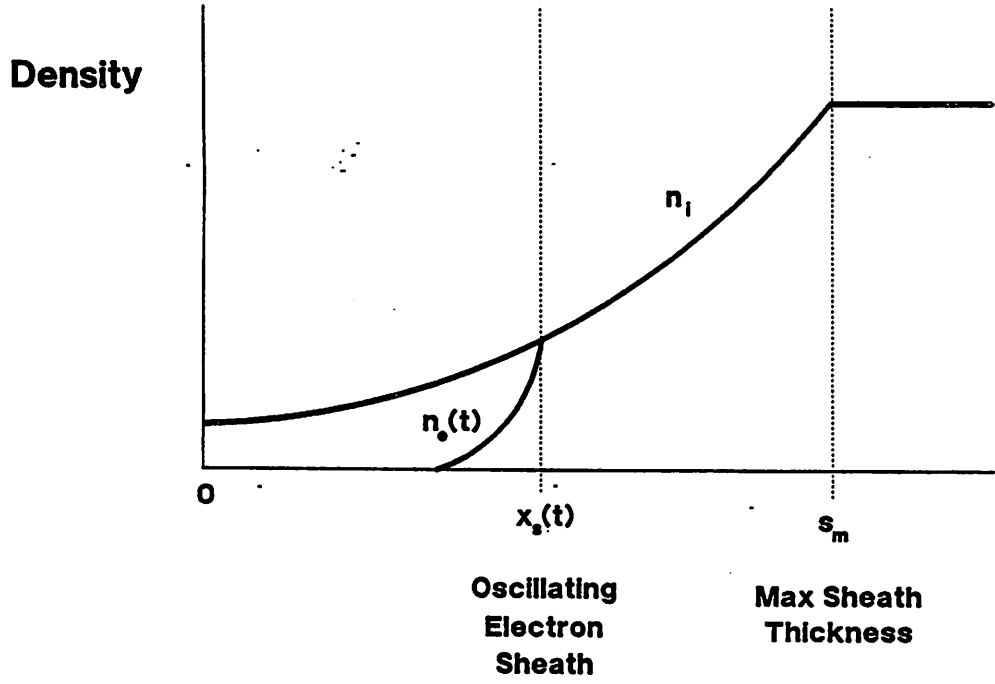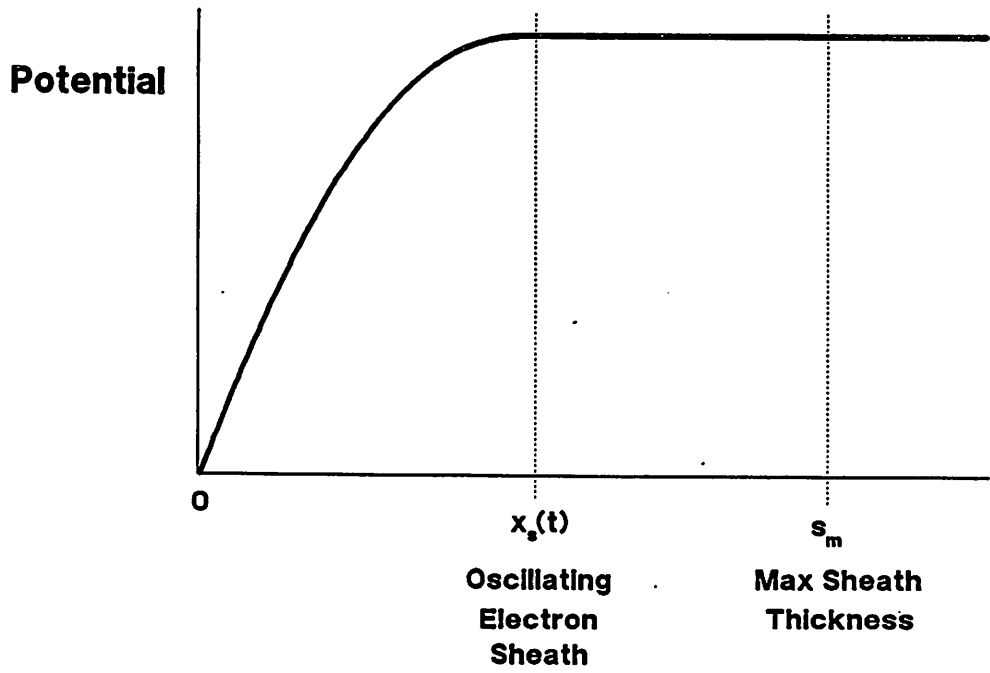
Figure 4

Figure 5

Figure 6

Figure 7

RMS Voltage of Probe (y-axis)

10^0

10^{-1}

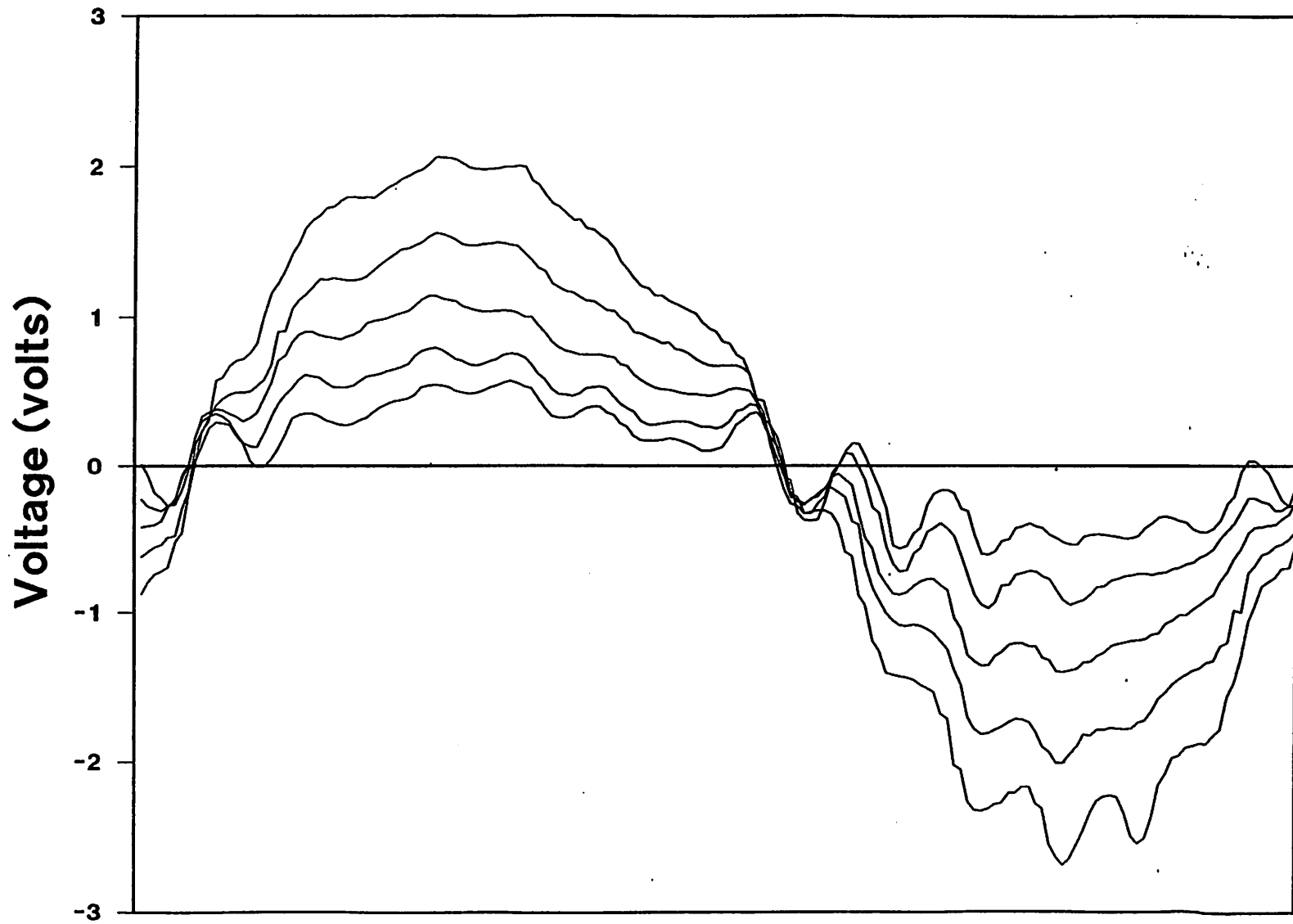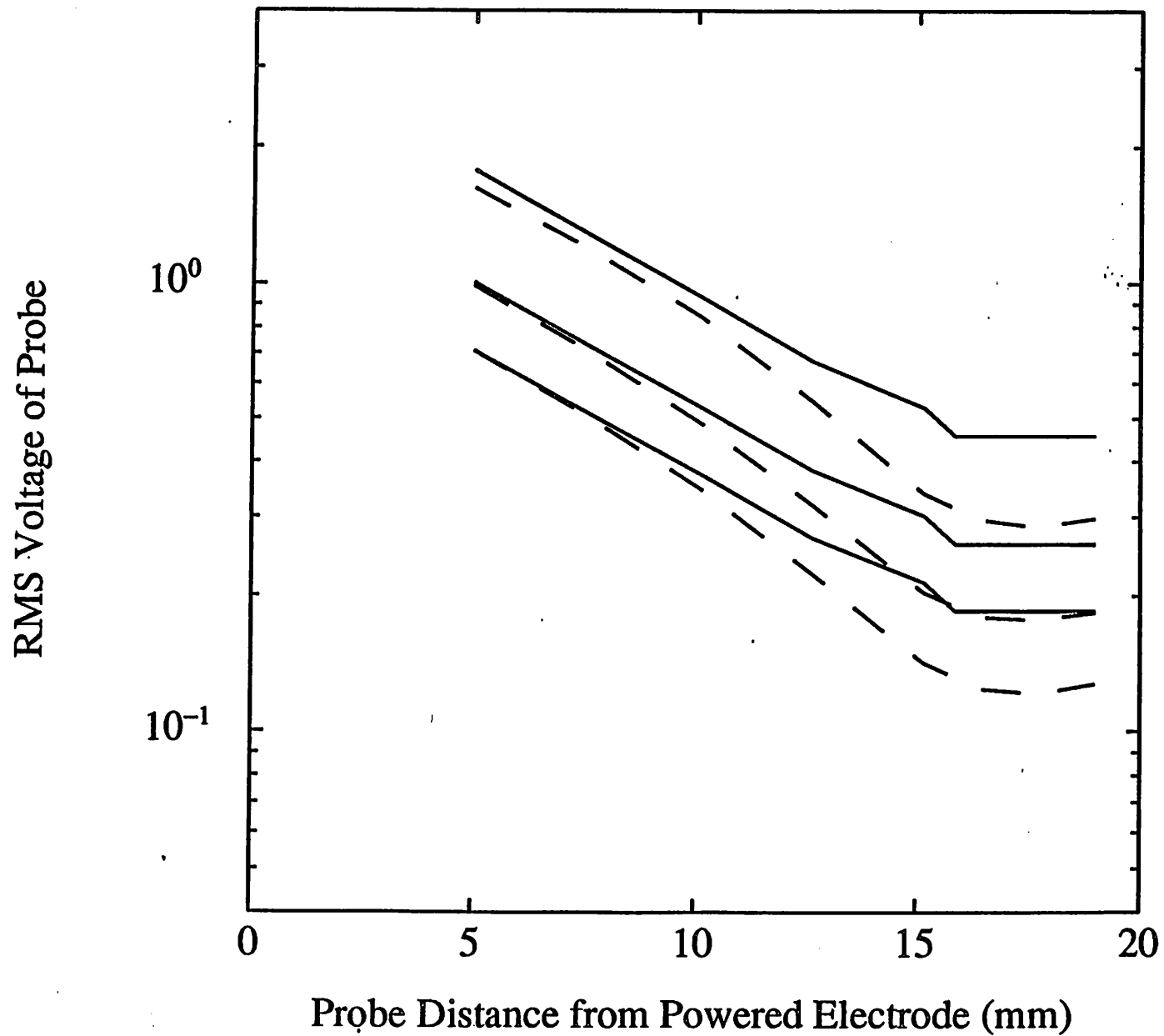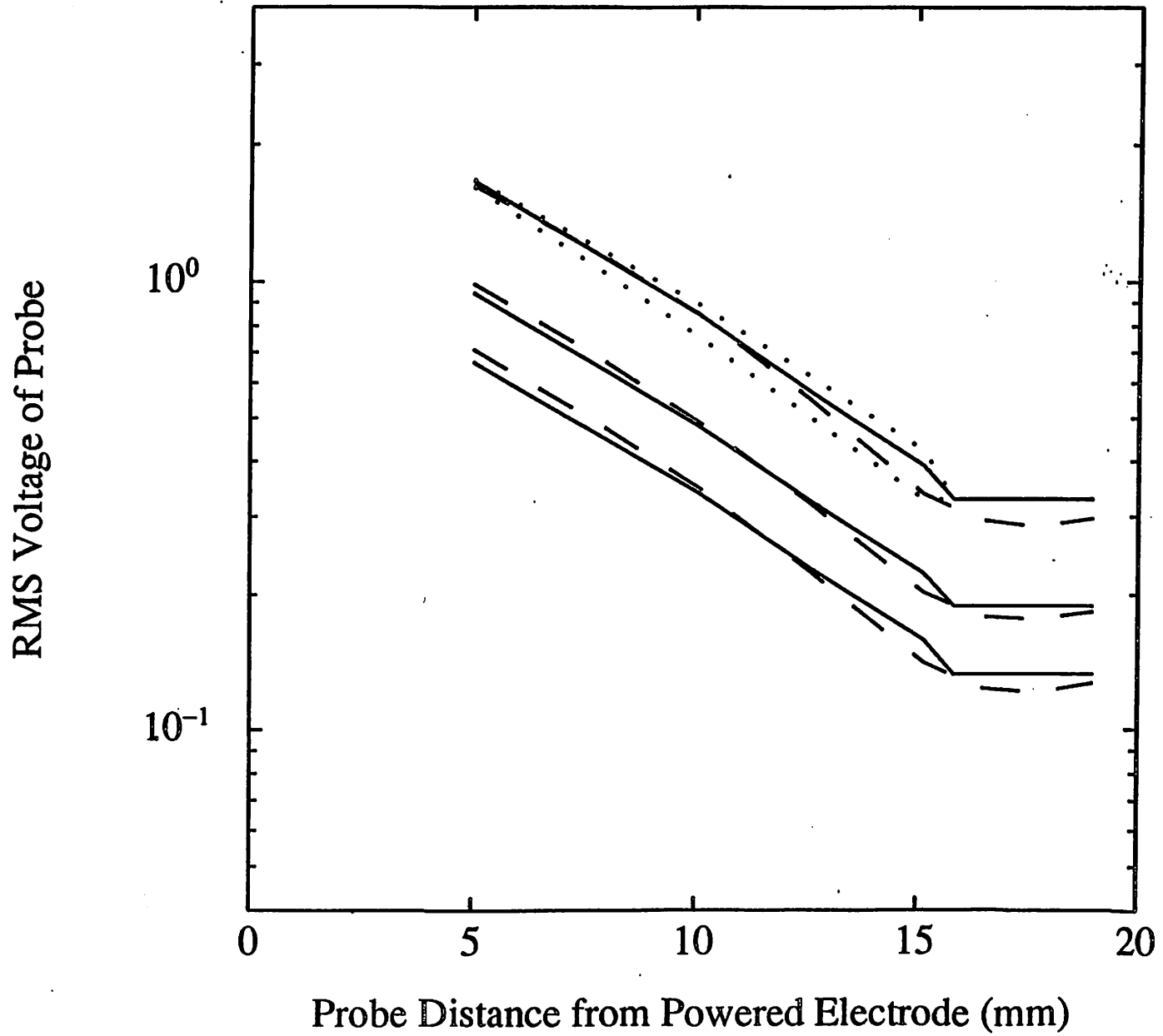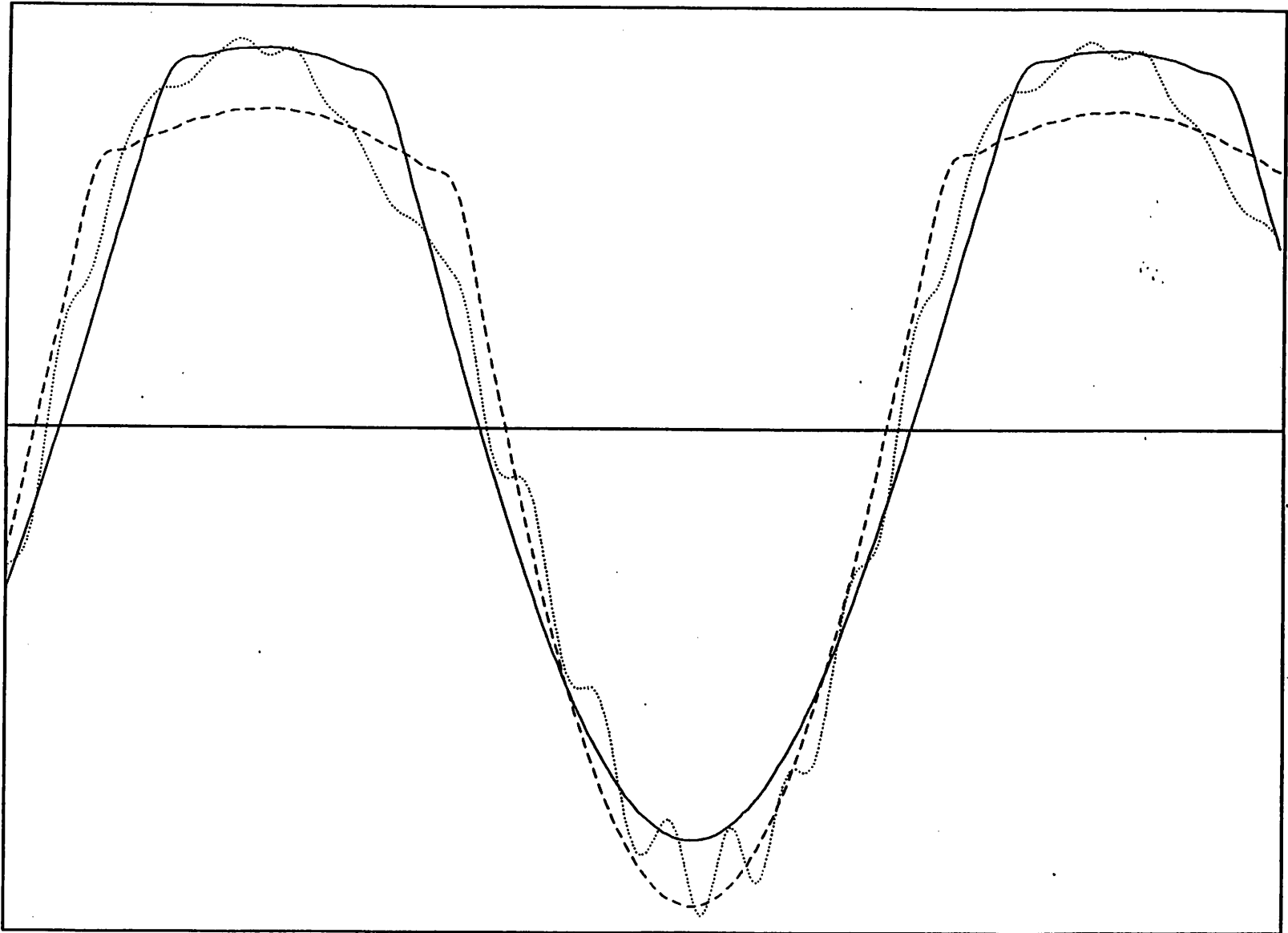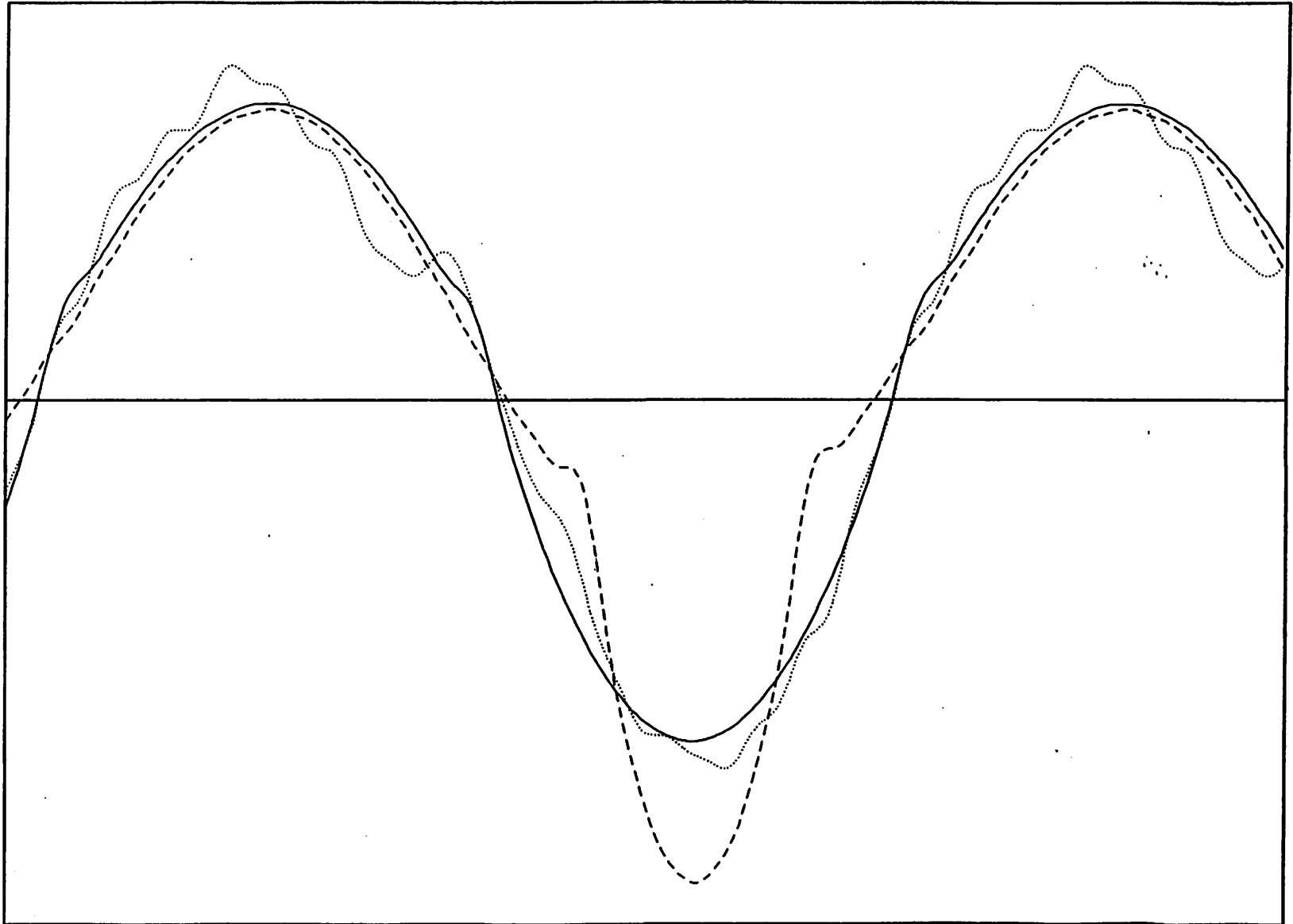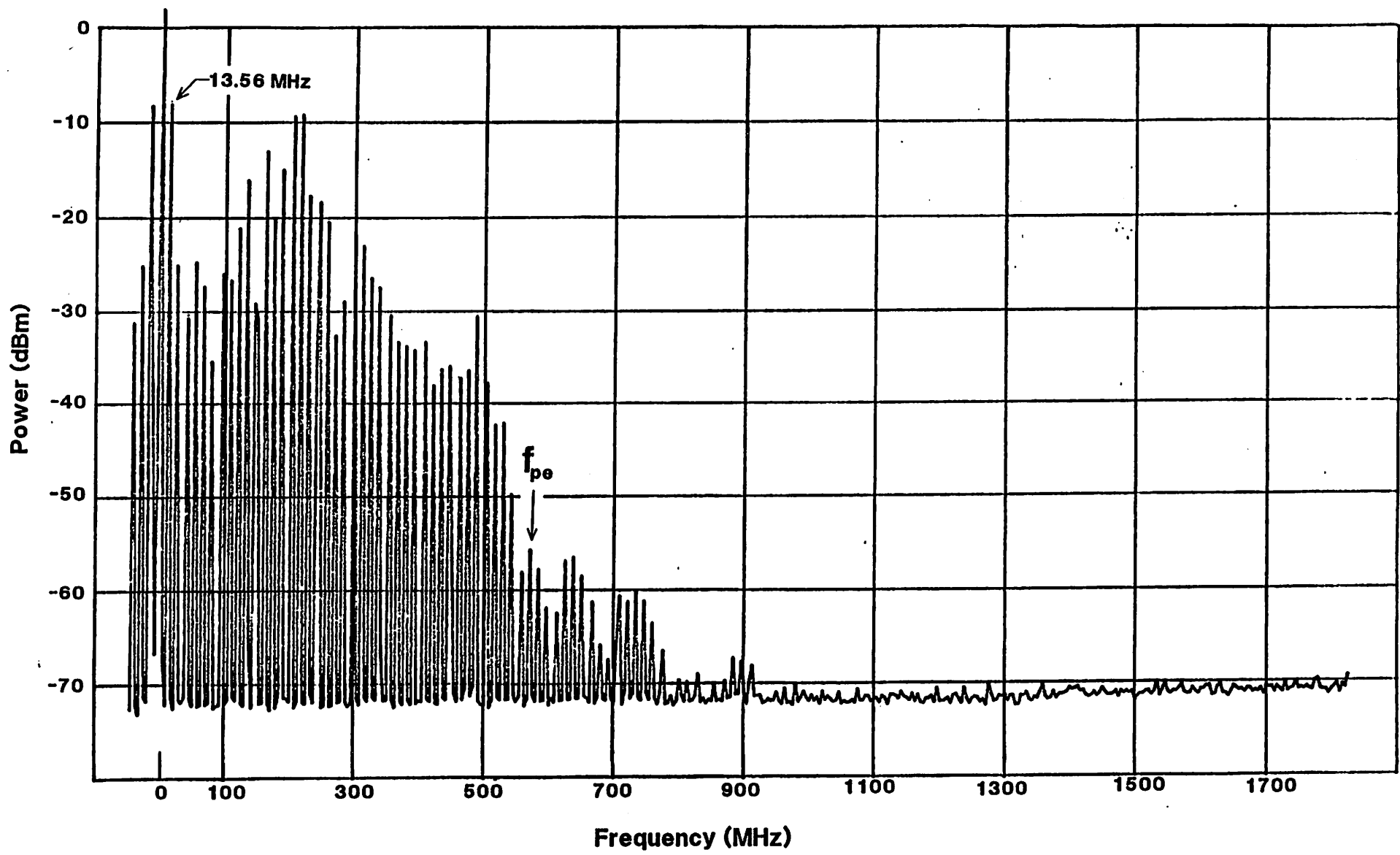**Probe Distance from Powered Electrode (mm)** (x-axis)
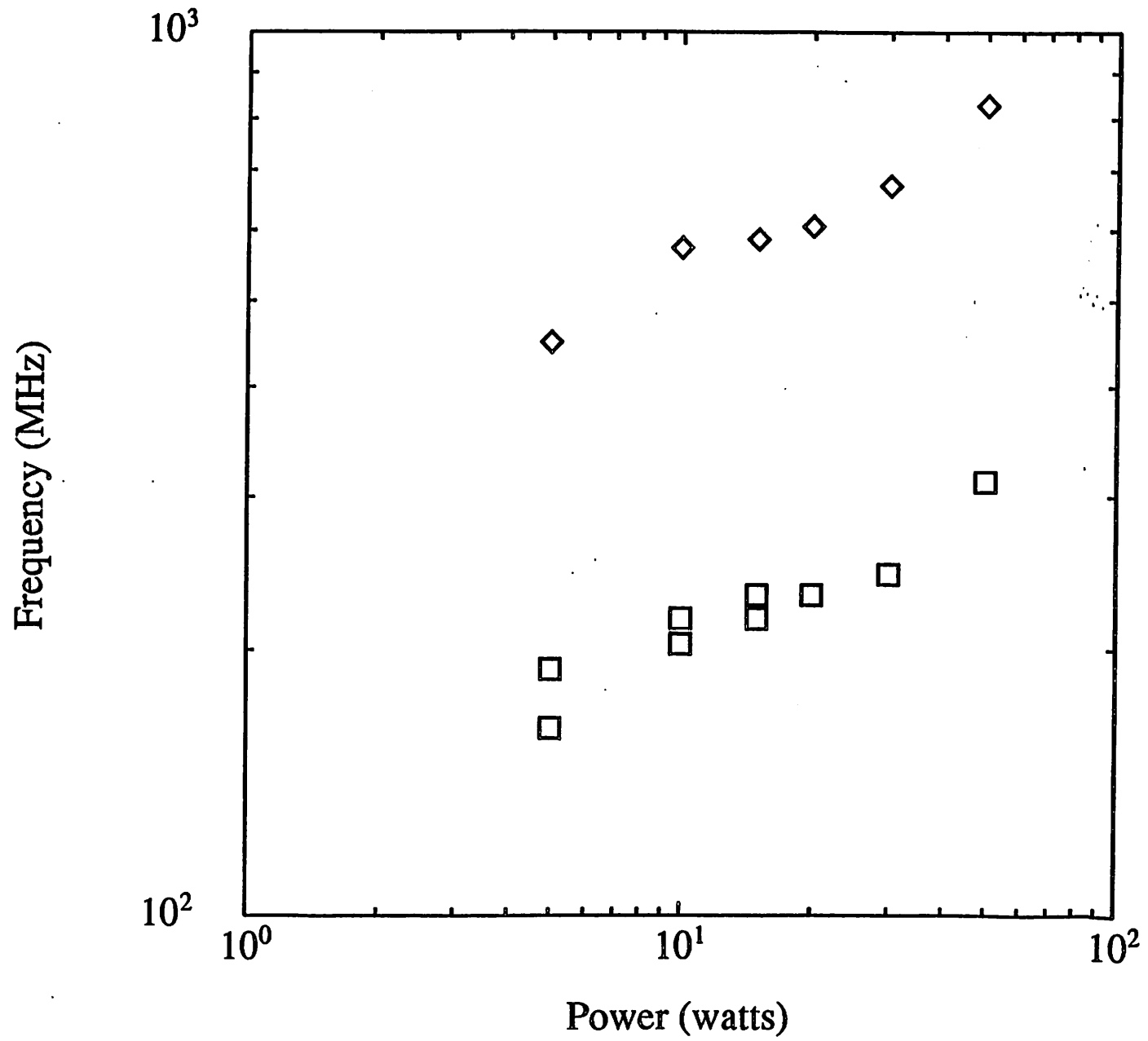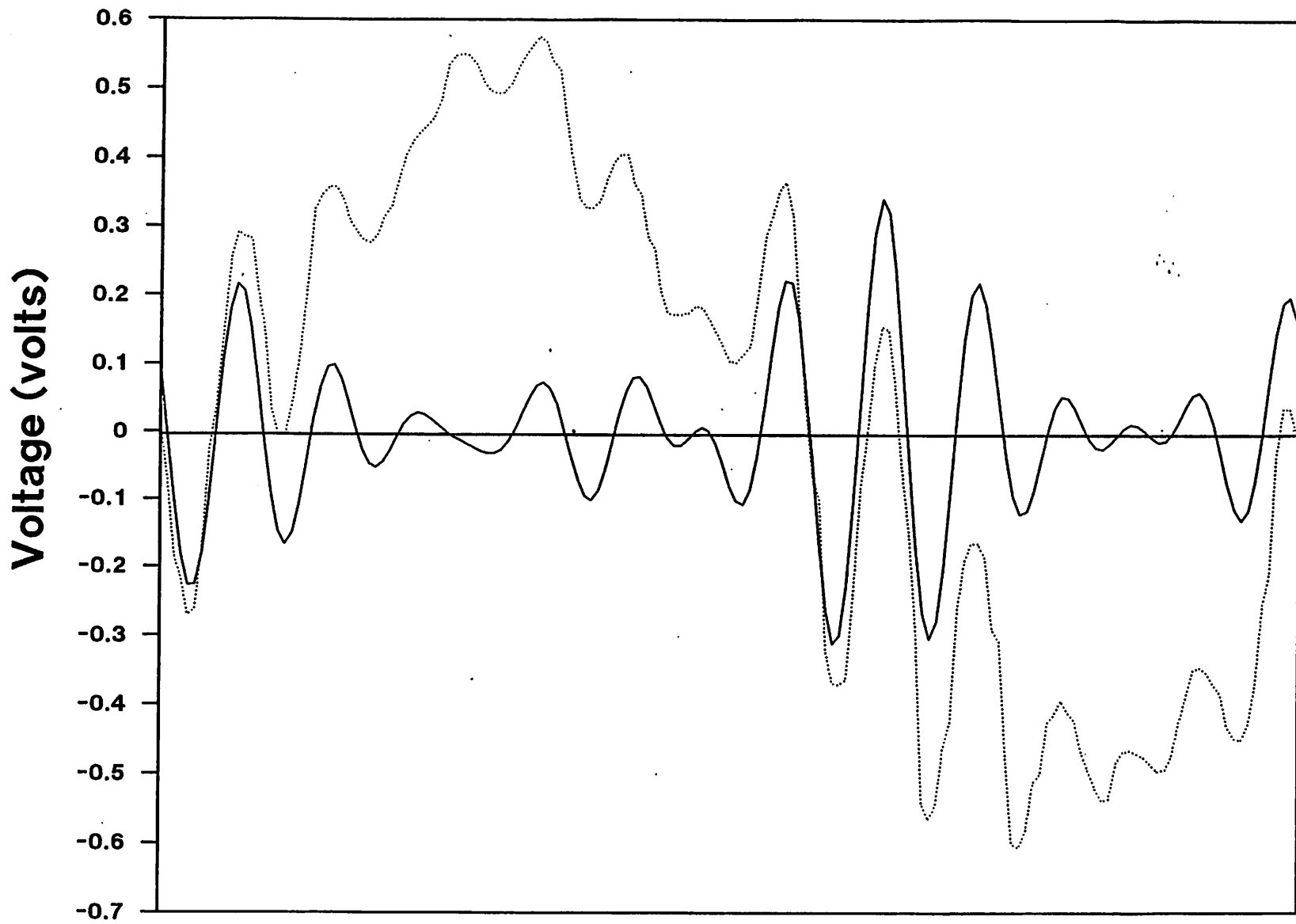
0   5   10   15   20

Figure 8

Figure 9

Figure 10

Figure 11

Figure 12

Figure 13

Figure 14